NOTICE

The quality of this microform is heavily dependent upon the quality of the original thesis submitted for microfilming. Every effort has been made to ensure the highest quality of reproduction possible.

If pages are missing, contact the university which granted the degree.

Some pages may have indistinct print especially if the original pages were typed with a poor typewriter ribbon or if the university sent us an inferior photocopy.

Previously copyrighted materials (journal articles, published tests, etc.) are not filmed.

Reproduction in full or in part of this microform is governed by the Canadian Copyright Act, R.S.C. 1970, c. C-30.

AVIS

La qualité de cette microforme dépend grandement de la qualité de la thèse soumise au microfilmage. Nous avons tout fait pour assurer une qualité supérieure de reproduction.

S'il manque des pages, veuillez communiquer avec l'université qui a conféré le grade.

La qualité d'impression de certaines pages peut laisser à désirer, surtout si les pages originales ont été dactylographiées à l'aide d'un ruban usé ou si l'université nous a fait parvenir une photocopie de qualité inférieure.

Les documents qui font déjà l'objet d'un droit d'auteur (articles de revue, tests publiés, etc.) ne sont pas microfilmés.

La reproduction, même partielle, de cette microforme est soumise à la Loi canadienne sur le droit d'auteur, SRC 1970, c. C-30.

Canada

Ion Pair Production and Electron loss of Fluorine and Chlorine Atom Collisions with Rare Gas Targets.

by

MUAZZAM W. ORAKZAÍ

Thesis submitted to the School of Graduate

Studies of the University of Ottawa in

partial fulfilment of the requirements

for the degree of Master of Science

in Physics

Physics Department

Faculty of Science

University of Ottawa

Ottawa, Canada

1988

ISBN 0-315-46835-1

UNIVERSITÉ D'OTTAWA
UNIVERSITY OF OTTAWA

ACKNOWLEDGEMENTS

I would like to express my sincere gratitudes to my thesis supervisor Dr. B. Hird for his encouragement, advice and help throughout the course of this work.

I would also like to thank Dr. F. Rahman for his assistance in some of the data collection and for general discussions.

Special thanks are due to my family and friends who gave me support and encouragement.

Finally, the financial assistance provided by the Government of Pakistan in the form of ST scholarship is gratefully acknowledged.

Contents

List of Tables

List of Figures

Chapter 1

Introduction

When two atomic particles in the keV range collide, a number of different processes may occur which produce fast neutrals and charged particles. For many years, astrophysicists focused their attention on ion-atom collisions. They tried to explain the spectroscopic observations and construct theoretical models of the stellar atmosphere.

Collisions between ions and atoms which lead to the ionization and excitation of atomic ions, detachment from negative ions, and the formation of the doubly charged ions, were considered for many years. Collision processes involving the destruction and the formation of negative ions have been investigated using charged and neutral beams of several keV, while at much lower energies, the determination of the threshold for charge transfer reactions and for ion-ion production in neutral-neutral collisions has yielded valuable information

about electron affinities. These investigations have scientific and practical importance. For instance, negative ions are employed in Tandem and other particle accelerators, and at TRIUMF.

In ion-atom collisions, one of the most extensively studied inelastic collision processes, and one which continues to be widely studied, is charge exchange. The practical importance of this process in many laboratories and astrophysical plasma has been recognized quite recently. For example, collision between multiply charged ions and atomic hydrogen are important in determining the radiation losses and neutral beam heating efficiencies in a fusion plasma, so that it contributes significantly to the energy and particle balance in the hot center of the plasma.

This thesis presents the measurements of the charge changing cross sections in neutral-neutral atom collisions. Table (1.1) describes a summary of the processes which can be identified separately.

1.1 Summary of the charge changing processes

$$A + B \rightarrow A^{+} + B + e - \Delta E \quad loss\ by\ ionization \tag{1.1}$$

$$A + B \rightarrow A^{\mp} + B^{\pm} - \Delta E \quad pair\ production\ by\ transfer \tag{1.2}$$

$$A + B \rightarrow A^{2+} + B + 2e - \Delta E \quad \textit{double loss by ionization} \qquad (1.3)$$

All these processes in neutral-neutral atom collisions are energetically possible at keV energies. The probabilities of these processes depend on the quasi-molecular structure of the interacting particles. An important parameter is the energy defect ΔE, which is the total change in the internal energies that take place during the collision. Its value can determine the magnitude of the cross section. The targets involved in the measurements reported in this thesis were all rare gas targets, which have no stable negative ions. Therefore electron transfer to the target cannot occur. The cross section of double ionization has been found experimentally to be very small, so it was neglected. Ion pair production which can be described in terms of single electron capture, and electron loss were therefore the dominant processes among those which were considered in the present experiments.

A new apparatus was designed to measure the ion pair production and electron loss cross sections. If the neutral beam is produced by positive ion neutralization, then it would probably contain a mixture of excited states, and it would be useless for cross section measurements because of the unknown mixture of the metastable states. Therefore a different method of neutral beam production was developed. The neutral beam was obtained by electron detachment during collisions between a previously accelerated negative ion beam within a

neutralizer gas. The advantage of this method is that it produces neutrals which are effectively all in the ground state.

The cross sections for the ion pair production and electron loss were measured as a function of projectile energy, by passing the neutral beam through a second region of low pressure, which was separated from the first neutralizer gas. This was called the target cell.

The equipment consists of two differentially pumped cylindrical gas chambers, each surrounded by vacuum. They were assembled as a single mechanical unit such that the neutralizer entrance and exit apertures formed a beam collimator for the target cell. The four apertures were carefully aligned. A clearing electric field between the two chambers was established across two parallel electrodes by an appropriate applied voltage, which removed the charged particles, so that only neutral particles reached the target cell in which the cross section were measured.

Measurements were taken in the projectile energy range from 10 to 110 keV for neutral fluorine and chlorine beams in collisions with all the rare gases. The systematic behavior of the cross sections were observed. With the fluorine beam, except for He and Ne, the cross section for negative ion production was found to increase with projectile energy and pass through a maximum, then decrease with increasing energy.

In chlorine, the single electron capture cross section was found to be energy dependent for all the targets except He and Ne. The cross section showed a significant broad peak at higher energies for heavy targets. The electron loss cross sections, both in fluorine and chlorine, were found to increase with energy and then decrease in the higher energy range. A maximum was found in the Cl-Ar electron loss cross section at about 80 keV energy.

The systematic errors of the cross section measurements were believed to be less than 10%. This estimate represents the sum of the individual errors arising from the target thickness corrections, pressure measurements, and the beam intensity fluctuations etc.

The mathematical details of the charge changing cross sections are described in Chapter 2. Chapter 3 and Chapter 4 outline the neutral beam production system and the experimental technique. Finally the results of the cross section measurements are discussed in Chapter 5.

Chapter 2

Mathematical Details

When a beam of particles collide with an atom or molecule of the target gas, the particle may capture or lose one or more electrons during successive collisions. The probability that a particular process occurs in a collision is conventionally expressed by its cross section. It is defined by the equation

$$dN = N_0 \sigma_{if} d\pi \tag{2.1}$$

where i and f represents the initial and the final states of charge i an f respectively. N_0 is the intensity of an assumed pure beam in state i before entering a target.

The target thickness π is the product of the length L of the target and n, the number of atoms per unit volume. This formula is defined under

conditions such that

$$\sum_f \sigma_{if} d\pi << 1 \tag{2.2}$$

so that only single scattering occurs, and $dN << N_0$, where dN is the intensity of the charge changed particles after the target.

The differential equation describing the transitions between possible charge states of a beam of particles, as they pass through a target gas of thickness π, is given by

$$\frac{dN^f}{d\pi} = \sum_{i \neq f} (\sigma_{if} N^i - \sigma_{fi} N^f) \tag{2.3}$$

where N^i is the fraction of the beam in charge state i, and N^f is the proportion of particles in state f.

We can include the term $i = f$ in the summation of equation (2.3), and we can write

$$\frac{dN^f}{d\pi} = \sum_i \sigma_{if} N^i \tag{2.4}$$

by defining

$$\sigma_{ff} = -\sum_{i \neq f} \sigma_{fi} \tag{2.5}$$

when the $\sigma\pi$ terms are small it is possible to expand N^f as a power series.

$$N^f = a_{0f} + a_{1f}\pi + a_{2f}\pi^2 + a_{3f}\pi^3 + ... \tag{2.6}$$

where $a_{0f} = N_0^f$ is the intensity with no target present, and therefore the incident intensity. Differentiating with respect to π, and substituting into equ.(2.3), we

get

$$a_{1f} + 2a_{2f}\pi + 3a_{3f}\pi^2 + ... = \sum_i \sigma_{if}(a_{0i} + a_{1i}\pi + a_{2i}\pi^2 + ...) \qquad (2.7)$$

now equating each power of π, we get

$$a_{1f} = \sigma_{if} a_{0i} \qquad (2.8)$$

or

$$= \sigma_{if} N_0^i \qquad (2.9)$$

$$2a_{2f} = \sum_k \sigma_{kf} a_{1k} \qquad (2.10)$$

or

$$a_{2f} = \frac{1}{2} N_0^i \sum_k \sigma_{kf}\sigma_{ik} \qquad (2.11)$$

and similarly

$$a_{3f} = \frac{1}{6} N_0^i \sum_l \sigma_{lf}\sigma_{fk}\sigma_{kl} \qquad (2.12)$$

By substituting the above equations into equation (2.6), we get

$$N^f = N_0^i + \sigma_{if} N_0^i \pi + \frac{1}{2}\pi^2 N_0^i \sum_k \sigma_{ik}\sigma_{kf} + ... \qquad (2.13)$$

The number of terms required depends on the target thickness. If $\sum \sigma\pi$ is a few percent, only a few terms are sufficient, but if each particle makes many collisions, many terms may be required for accuracy. Since the projectile beam used in the present experiments was neutral , $i = 0$. If we consider electron

transfer as defined in equation (1.2), then $f = +1$, and equation (2.13) can be written as

$$N^+ = N_0^0 \sigma_{0+} \pi \left[1 + \frac{1}{2}(\sigma_{00}\sigma_{0+} + \sigma_{0+}\sigma_{++} + \sigma_{0-}\sigma_{-+} + \sigma_{02}\sigma_{2+})\pi \right] \tag{2.14}$$

where, from equation (2.5)

$$\sigma_{00} = -(\sigma_{0+} + \sigma_{0-} + \sigma_{02}) \tag{2.15}$$

and

$$\sigma_{++} = -(\sigma_{+0} + \sigma_{+-} + \sigma_{+2}) \tag{2.16}$$

In equation (2.14) we assume that the target is thin enough that one can neglect terms of higher order than $(\sigma\pi)^2$ in the expansion of equation (2.13). In the measurement $(\sigma\pi)$ is of the order of a few percent. The neutrals which remain unchanged after the target correspond to $f = 0$, and equation (2.13) becomes

$$N^0 = N_0^0 \left[1 + \sigma_{00}\pi + \frac{1}{2}(\sigma_{0-}\sigma_{-0} + \sigma_{0+}\sigma_{+0} + \sigma_{00}^2)\pi^2 \right]. \tag{2.17}$$

Equations (2.14) and (2.17) give the intensities of the neutrals and positives after the target in terms of the intensity N_0^0 of an initially pure neutral beam. Dividing equation (2.14) by (2.17), and keeping terms of order π in the large brackets,

$$N^+ = N^0 \sigma_{0+} \pi \left[1 - \frac{1}{2}\sigma_{00}\pi + \frac{1}{2}(\sigma_{++} + \frac{\sigma_{0-}\sigma_{-+} + \sigma_{02}\sigma_{2+}}{\sigma_{0+}})\pi \right] \tag{2.18}$$

The ratio of positives to neutrals after the target can be obtained by dividing

equation (2.18) by (2.14), to obtain

$$\pi\sigma_{0+} = \frac{N}{1+\frac{1}{2}N}\left[1+\frac{1}{2}(\sigma_{+0}+\sigma_{+-}+\sigma_{+2}-\sigma_{0-}-\sigma_{02}-\frac{\sigma_{0-}\sigma_{-+}+\sigma_{02}\sigma_{2+}}{\sigma_{0+}})\pi\right] \tag{2.19}$$

where N is defined as N^+/N^0. The incident beam intensity N_0^0 has been eliminated and the cross section can be determined experimentally, using equation (2.19) , from measurements of the charge ratio N after the target, as a function of the target thickness π.

If we substitute $f = -1$ in equation (2.13), and repeat the calculations, the expression becomes

$$\pi\sigma_{0-} = \frac{N}{1+\frac{1}{2}N}\left[1+\frac{1}{2}(\sigma_{-0}+\sigma_{-+}+\sigma_{-2}-\sigma_{0+}-\sigma_{02}-\frac{\sigma_{0+}\sigma_{+-}+\sigma_{02}\sigma_{2-}}{\sigma_{0-}})\pi\right] \tag{2.20}$$

where N is now defined as N^-/N^0 which is the general form for the single pair production cross section to second order in π. The right sides of equations (2.19) and (2.20) represent the correction terms for finite target thicknesses. When the target is very thin, so that $N << 1$ and $(\sigma\pi) << 1$ both simplify to $\pi\sigma_{0\pm} = N$

Chapter 3

Experimental Arrangement

3.1 General Description

The technique used for the measurement of the charge changing cross sections is an extension of that previously [1] used for negative ion-atom collision studies. The equipment and the newly designed apparatus for producing an incident neutral fluorine and chlorine beam are described briefly in this section. It is convenient to classify the experimental arrangement in the following three sections.

- Beam Preparation
- Magnetic Analyzer
- Collision Chamber

3.2 Beam Preparation

Generally, the production of a suitable beam for performing the collision studies is a relatively simple matter. Radio frequency ion sources have been utilized for many years to produce ions for use in charge transfer cross section measurements. A conventional type of radio frequency ion source consists of a glass tube surrounded by the coil of a high frequency oscillator, to produce a plasma discharge.

An electric field was maintained to a few kV potential between the anode and the exit canal. The discharge tube gas pressure was controlled by a thermal mechanical leak in the range of about 10^{-2} to 10^{-4} Torr. This device, consists of a polished steel ball of 3 mm diameter which is pressed against a small hole of 2 mm diameter by the tension in a wire. An electrical heater, wound round the wire, controls the tension by thermal expansion and so controls the gas flow rate round the ball into the hole. The positive ions were extracted from the plasma boundary by the strong electric field and were accelerated towards a narrow metal exit tube, called the canal. Inside the canal, the negative ions were produced from the positive ions by electron capture collisions with the residual gas there, and these negative ions were pulled into the accelerator column by the reversed potential of the extractor electrode.

The production of negative ions by this method has the advantage that they are not accompanied by large numbers of electrons. The most convenient gas for producing both fluorine and chlorine was found to be commercial available Freon-12 (CCl_2F_2), which gave no unusual contamination. The negative ions were accelerated to the desired energy by a 150 kV accelerator (Model 150,Texas Nuclear Corporation).

The total length of the beam line was about 10 meter from the accelerator to the collision chamber. A good vacuum was achieved by four diffusion pumps backed by one rotary pump, and located at different positions along the beam line. The working pressure throughout the beam line was kept to about 5×10^{-6} Torr.

The general assembly of the beam line from the accelerator to the collision chamber is shown in figure (3.1). Two sets of magnetic steerers were located just after the accelerator to make small adjustments of the beam position and direction before the magnetic analyzer. A third steerer was used to optimize the beam through the neutralizer and target. At about 4 meter from the accelerator an adjustable aperture was used to set the beam current during the measurements. Negative ion currents striking the first aperture of the neutralizer cell were typically 10^{-10} A.

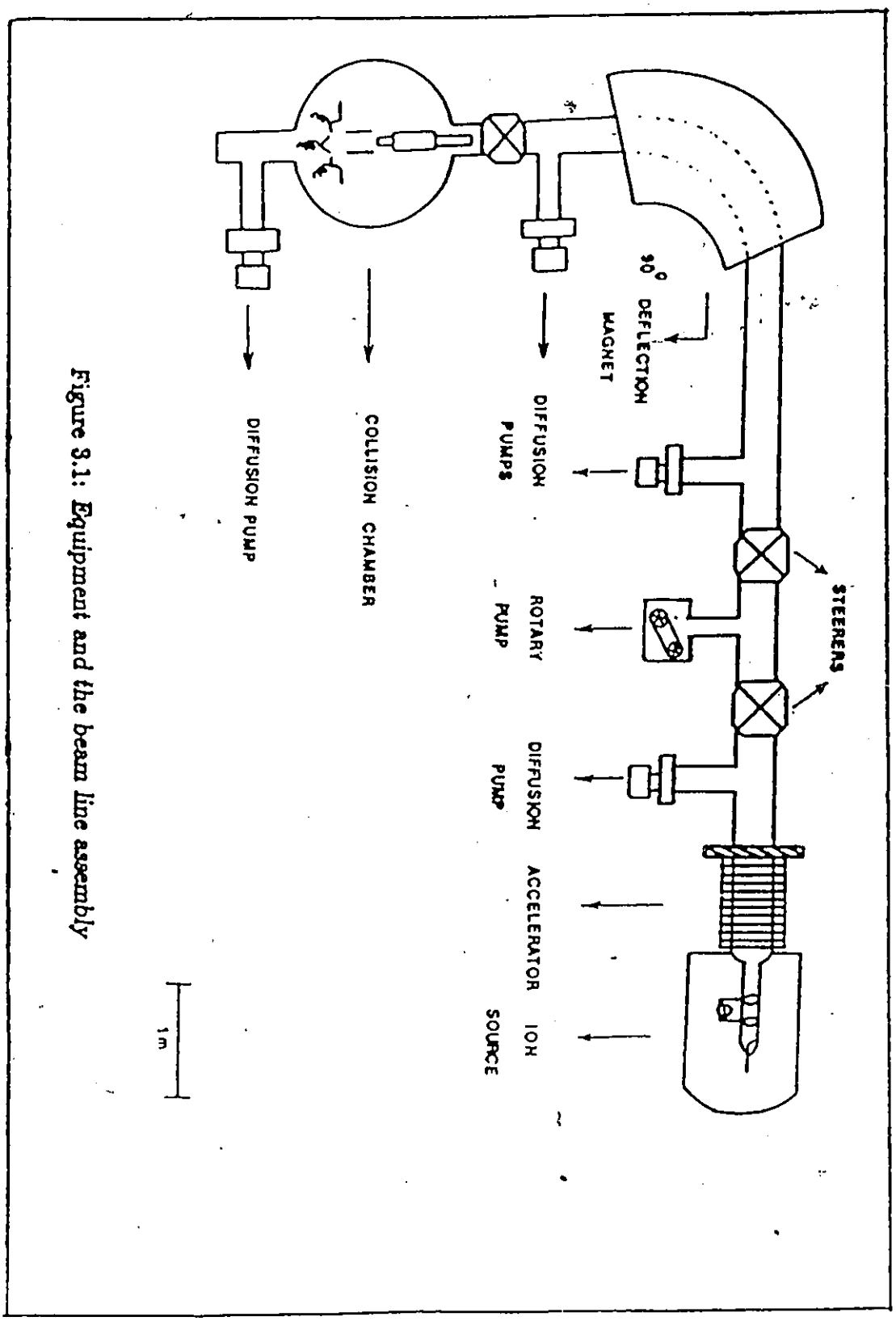

Figure 3.1: Equipment and the beam line assembly

3.3 Magnetic Analyzer

The beam from the ion source usually contain a mixture of different species of ions. In order to select the particles of the chosen mass from a beam, a technique of magnetic analysis was applied which separates out the components of different momentum and selected one of the discrete mass beams. In the present experiment, the projectile beam from the ion source was analyzed by a double focussing, 90^0 deflection and 66 cm radius uniform magnetic analyzer (HV Engineering Corporation,Model 90-26).

In a uniform magnetic field, the radius of curvature is proportional to the momentum of the particle and is given by

$$r = \frac{mv}{Bq}, \tag{3.1}$$

where the velocity v is given by

$$v^2 = \frac{2qV}{m}, \tag{3.2}$$

where the ion energy is qV, and V is the accelerating voltage. Substitution of equation (3.2) into (3.1) gives

$$Br = \left(\frac{2mE}{q^2}\right)^{\frac{1}{2}}, \tag{3.3}$$

where E is the ion energy $E = qV$. Therefore

$$\frac{mE}{q^2} = \frac{1}{2}B^2r^2. \tag{3.4}$$

Since we have a constant radius of curvature for all the ions which traverse the magnet and reach the neutralizer, one can write equation (3.4)

$$\frac{mE}{q^2} \propto B^2. \tag{3.5}$$

If the magnetic iron is magnetically soft and does not saturate, the field B is nearly proportional to the magnetic current I in the magnetic coil windings.

In order to minimize the hysteresis effects, the data were always taken when the current was changing in one direction (increasing). All ions should therefore lie on the same line of a graph where mE/q^2 is plotted as a function of I^2, as shown in the figure (3.2). Sufficient number of points were determined , using the most abundant ions, with both positive and negative charges, at several energies, so that the line was clearly determined. A mass spectrum is shown in the figure (3.3), where fluorine and chlorine were identified and table (3.1) gives a proposed identification of peaks of various singly charged ions.

Figure 3.2: *Mass calibration of singly charged ions*

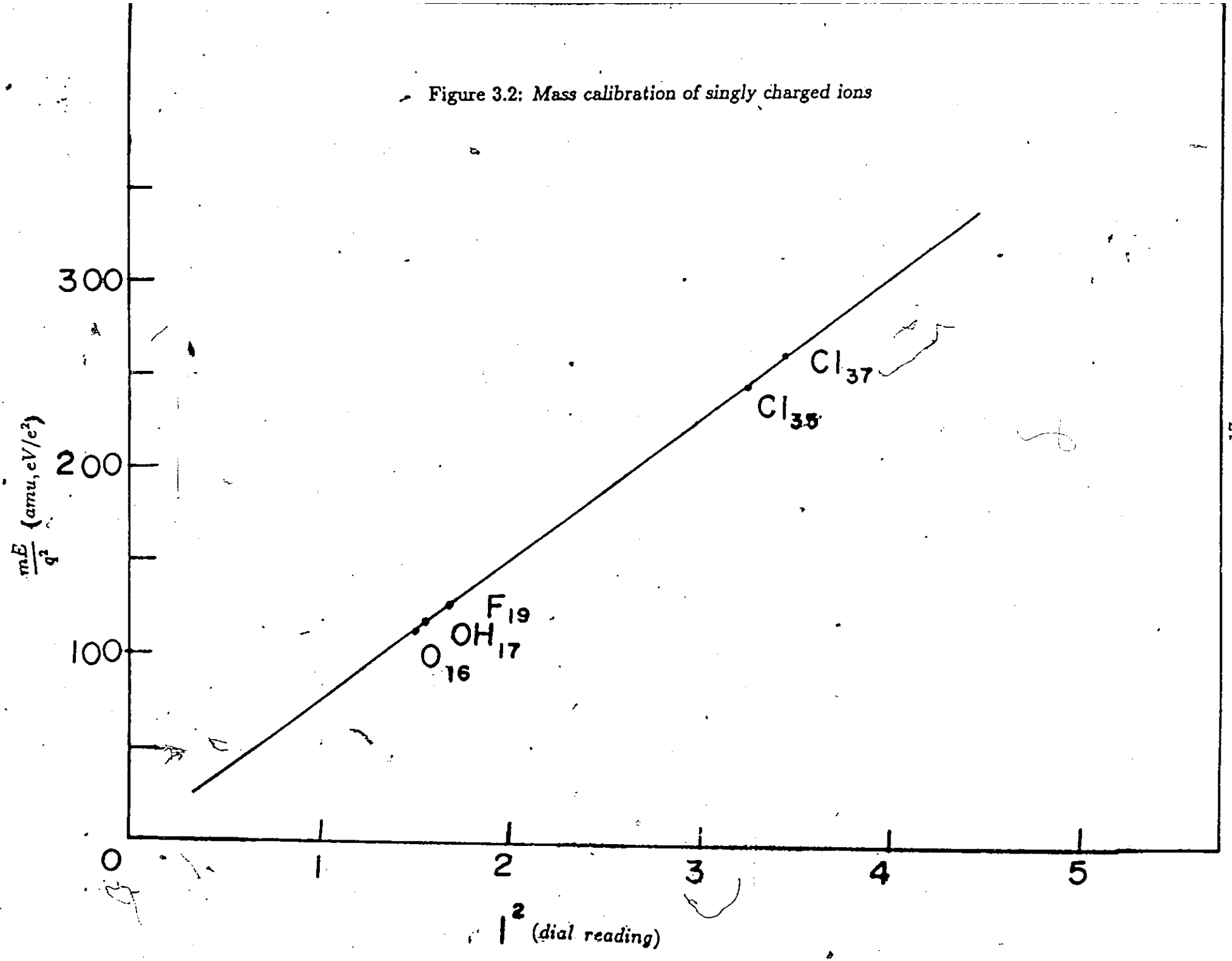

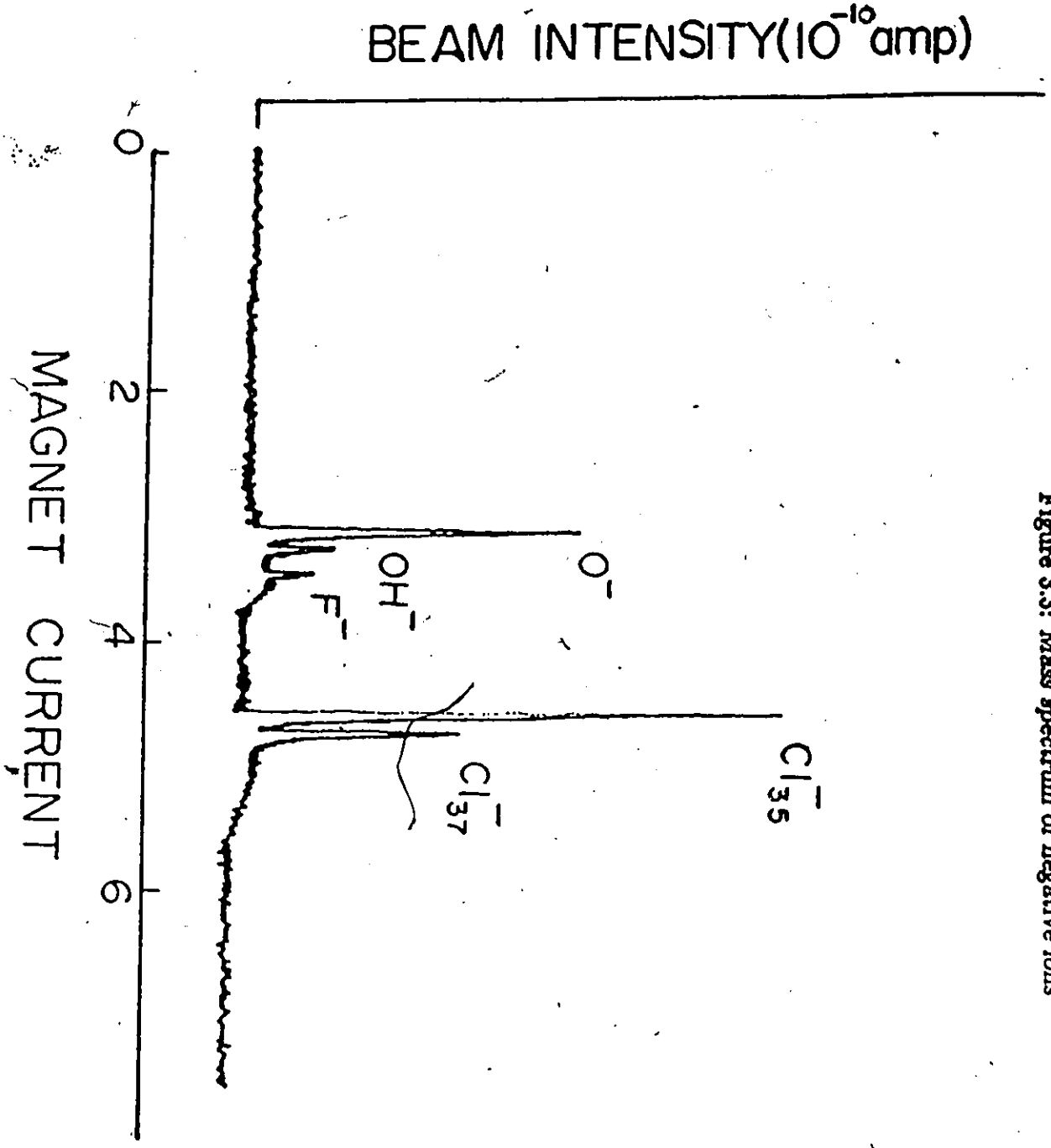

Figure 3.3: *Mass spectrum of negative ions*

Mass (a.m.u)	$I^2(dial\ reading)$	$\frac{mE}{q^2}(amu, eV/e^2)$	Proposed Species
16	1513	1120	O^-
17	1557	1190	OH^-
19	1656	1330	F^-
35	3249	2450	Cl^-
37	3445	2590	Cl^-

Table 3.1: *Mass spectrum identification of singly charged ions.*

3.4 Collision Chamber

A previously designed vacuum chamber has a cylindrical geometry with 15 cm height and 36 cm in diameter. In addition to some other internal changes, a newly constructed assembly of the neutral producing system and the target gas cell was installed inside the vacuum chamber. A photograph, shown in figure (3.4), provides a view of the internal geometry of the collision chamber.

The schematic layout of the beam collimator is shown in figure (3.5) and the design of the neutralizer and the target gas cells is shown in figure (3.6). The assembly consists of a 19 cm long brass cylinder. It was threaded at each end, and into it were screwed two aluminum cylindrical gas cells, the neutralizer and the target cell. The machiniry was carefully done so that all these cylinders were accurately on the same axis. Into the ends of the aluminum

cylinders were installed ceramic plates to which brass discs were attached. Thus providing insulated apertures, so that the beam currents could be monitored for alignment. The whole system was mounted on the common base plate of the collision chamber with two adjustable-V-shaped blocks mounted on three ball bearings in machined grooves. The design of this equipment was made such that it could be disassembled and reassemble again in exactly the same position. Photographs of this apparatus are shown in figures (3.7) and (3.8). The vacuum surrounding the neutralizer and target gas cell was kept at 5×10^{-6} Torr by pumping the whole chamber.

The equipment inside the chamber consisted of the following three components.

- Neutral Producing System
- Target Gas Cell
- Channel Electron Multiplier

Figure 3.4: *Photograph of the collision chamber.*

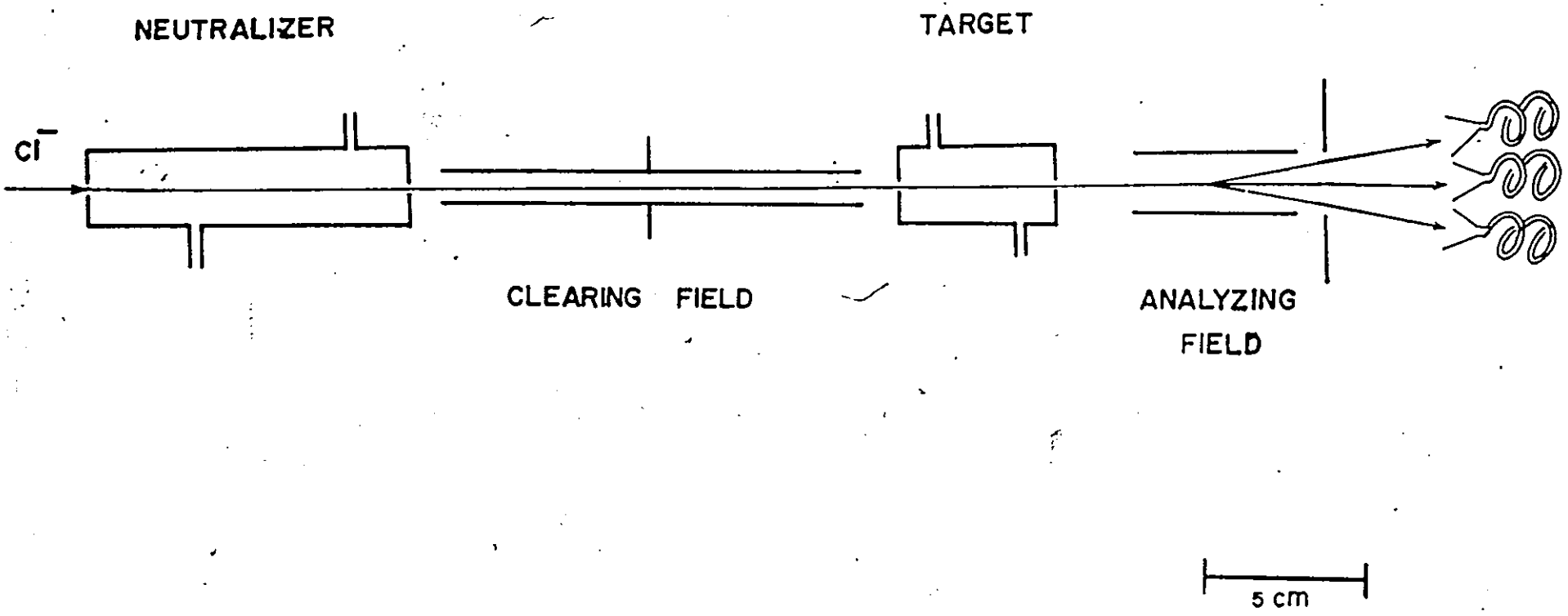

Figure 3.5: *Schematic layout of the neutralizer and target gas cells.*

Figure 3.6: *Neutral producing apparatus.*

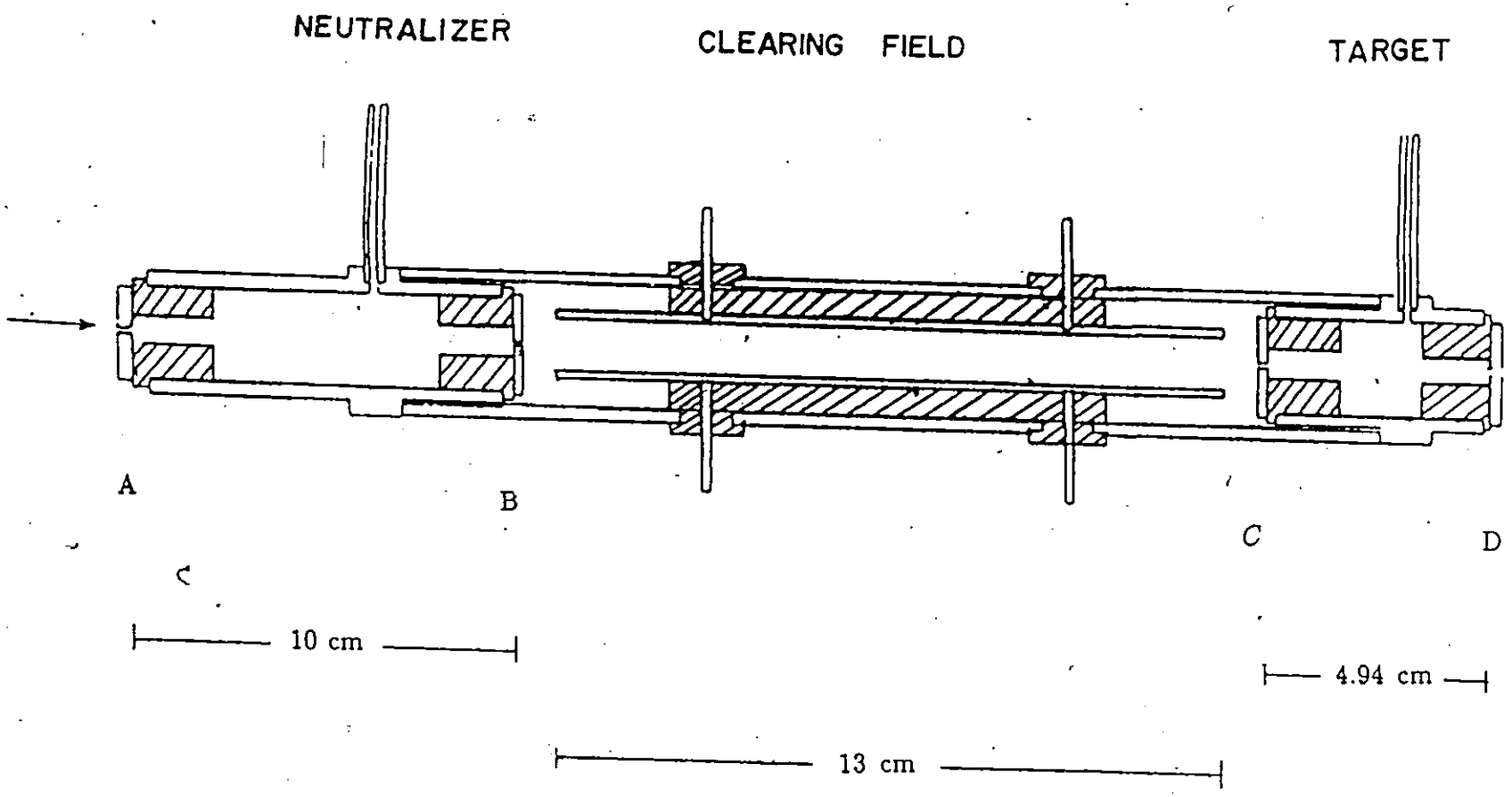

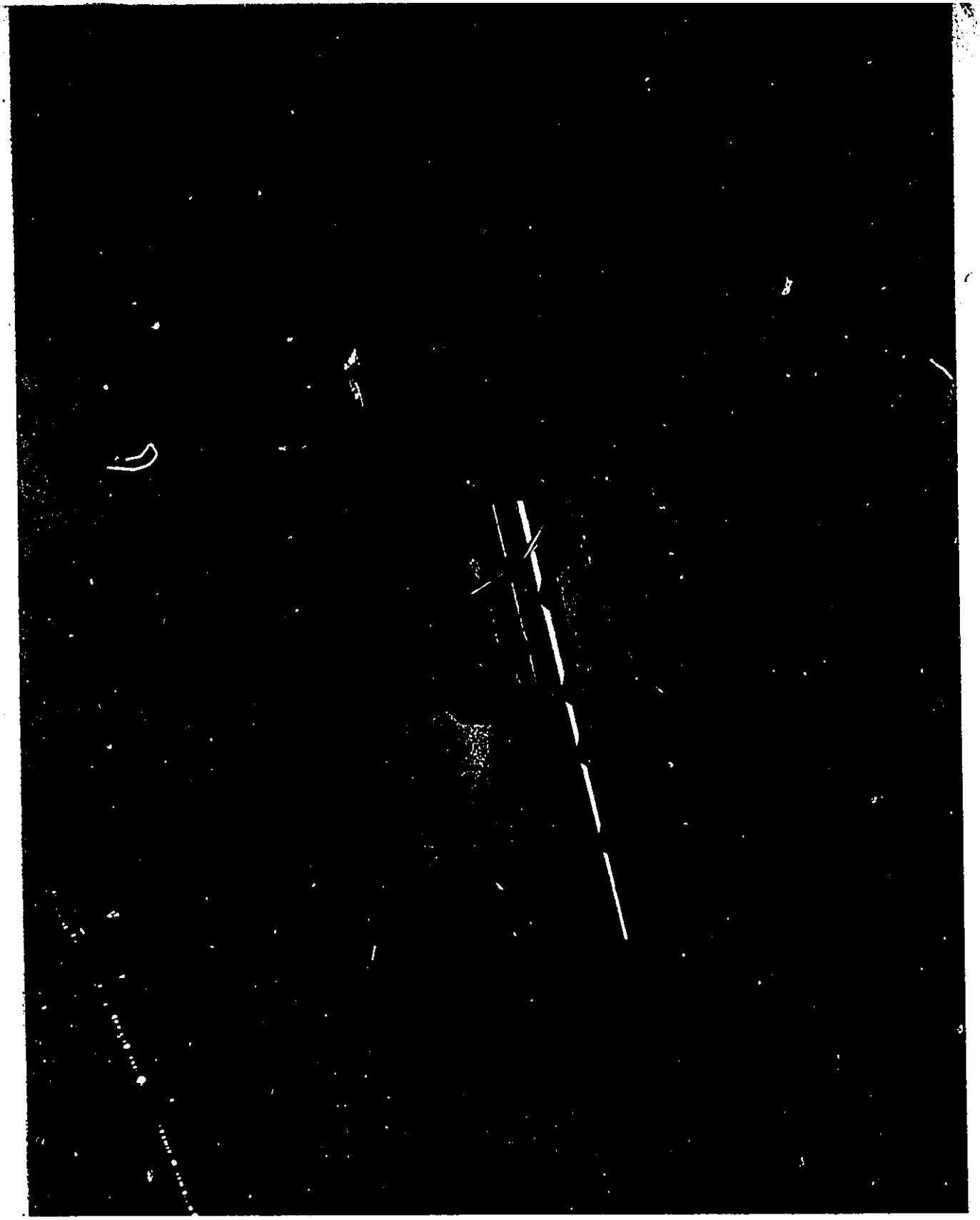

Figure 3.7: *Photograph of the neutral producing system.*

Figure 3.8: *Clearing field of the neutralizer gas cell.*

3.5 Neutral Producing System

The neutral producing system consisted of a neutralizer gas cell and a clearing electric field. The neutralizer was 10 cm long with two insulated apertures at either end. The slit A of 0.8 mm diameter serves at the entrance and slit B of 0.65 mm diameter was at the exit of the cell. Beyond this, inside the central brass cylinder, two parallel electrodes 13 cm long were used to produce the transverse clearing field to sweep away the negative and positive charged components in the beam.

Before taking the actual measurements of the σ_{0+} and σ_{0-} cross sections, some preliminary tests were made to chose a suitable gas for the neutralizing cell. A number of different gases were tried in the cell and the charge ratio of neutral and charge components were determined as a function of the gas pressure in the cell. When comparing oxygen, nitrogen and argon, it found that each gas was able to produce 60% neutrals from the negative projectile beam. Figure (3.9) indicates the ratio of negative count as a function of neutralizer gas pressure. To reduce the effects of contamination of the target gas with a neutralizer gas having a very different cross section, it was decided to use argon for the neutralizer. The working pressure in the neutralizer was maintained at 10^{-3} Torr, which was monitored continuously by a capacitance manometer (MKS BARATRON).

Figure 3.9:

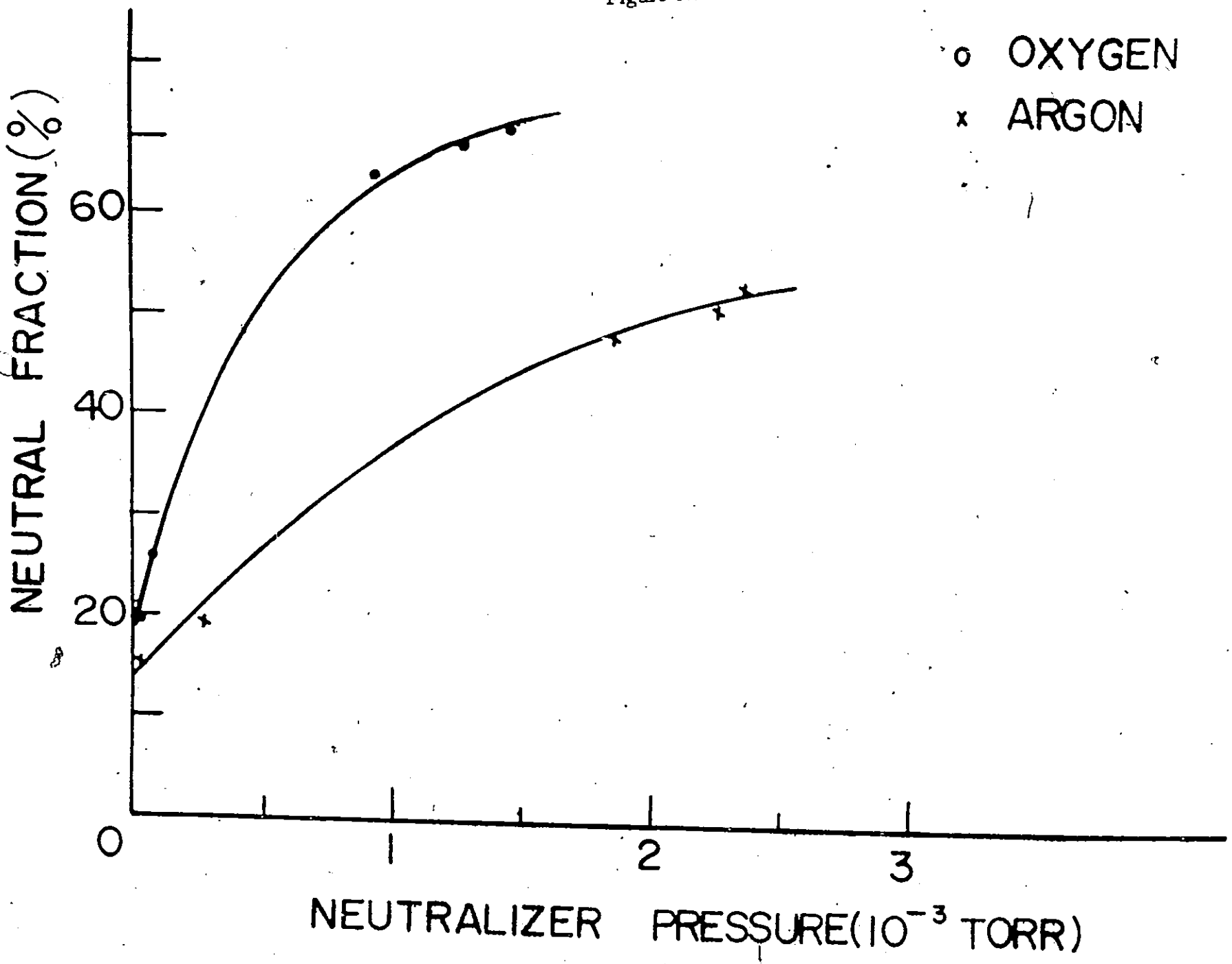
o OXYGEN
x ARGON
NEUTRAL FRACTION (%)
0
20
40
60
1
2
3
NEUTRALIZER PRESSURE(10^{-3} TORR)

An electric field of about 250 V/cm was found to be the minimum necessary for the removal of charged particles from the incoming beam. Tests were carried out with different clearing electric fields from 250 V/cm to 400 V/cm. Table (3.2) shows the result of a test of the neutralizer in which both the pressure and the clearing electric field were changed at different energies.

It was verified that no significant change was found in the measured cross section values when the neutralizer pressure was increased or decreased from 0.4×10^{-3} Torr to 2.5×10^{-3} Torr. At the high end of the energy range, when the clearing electric field was increased up to 400 V/cm at constant pressure, the measured values of the cross section were found to be reduced by 1 to 2%, which is not statistically significant.

A similar check was done for a positive beam incident on the neutralizer gas, when clearing field was increased at constant pressure. The cross section value changed by not more than 3% from the value obtained with the negative ion beam. At low energies, when the beam intensity was small, a pressure of 3×10^{-3} Torr was used so as to obtain more intense neutral beam.

E (keV)	$P(Torr)$	$Clearing\ field(V/cm)$	$\sigma_{0-}(10^{-16}cm^2)$	$\sigma_{0+}(10^{-16}cm^2)$
45	0.4×10^{-3}	250	4.97	1.91
45	2.5×10^{-3}	250	5.03	1.97
81	9×10^{-4}	250	5.81	2.76
81	9×10^{-4}	400	5.60	2.70

Table 3.2: *Neutralizer Pressure and clearing electric field.*

3.6 Target Gas Cell

The target cell was situated beyond the clearing electric field. It consisted of an aluminum cylinder with insulated apertures. It was 4.94 cm long with a 0.43 mm diameter entrance and a 1.5 mm diameter exit aperture. In order to avoid slit generated ions from being counted, the target exit aperture was made wider than the other apertures, so that with the accurate alignment, it was out of the direct neutral beam. The dimensions of the target gas cell were chosen such that a few percent of the atoms made single collisions, and therefore double collisions were of the order of a few percent of the single collisions , and higher order collisions were completely negligible.

The target gas cell was connected by two copper pipes, one was connected to the thermal mechanical leak and the other to the capacitance manome-

ter, which measured the gas pressure in the cell. The thermal mechanical leak controlled the gas flow to the target cell. The pressure in the cell was allowed to stabilize before each measurement.

At a distance of 2.5 cm beyond the target exit aperture, an electrostatic deflector was used for separate the charge states of the beam leaving the target. It was mounted on the common base plate of the vacuum chamber. It consisted of two parallel plates, separated by 1.5 cm and each of length 5 cm. Deflecting voltages of about 4 kV were required to deflect beams of more than 80 keV. The field emission then became a problem. A solution was found by using a 2.5 cm long aluminum shield with 1 cm window which was attached to the deflecting plates just in front of the detectors. This shield reduced the field emission electrons which reached the channeltrons without obstructing the paths of those particles travelling from the target to the detectors.

3.7 Channel Electron Multiplier

The electrostatic deflector separated the charge components of particles emerging from the target cell. Three channel electrons multipliers (channeltrons) were used as particle detectors to count these different charge state particles simultaneously. They were placed side by side at a distance of 13 cm from the target cell, which made it possible to collect all those particles which were

scattered into a 2^0 cone. The geometry of the collision chamber, including the neutral producing system and channeltrons was made carefully such that the scattered particles were incident upon the cone of the appropriate channeltron entrance aperture.

Basically, a channeltron is a nonmagnetic device fabricated from a special kind of glass. Its interior surface is coated with a conducting material which serves as a continuous dynode. The current pulse from an incident particle is increased by secondary electron multiplication. A potential of up to 3 kV is applied across the ends of channel. Channeltrons must be operated in a vacuum environment of less than about 10^{-5} Torr to avoid ionization of the residual gas inside the tube.

Channeltrons are of various types, depending upon their design and use. In the present experiment, charge particles as well as neutrals were detected by two kinds of channeltrons. The neutral particle counter was B419BL01 Philips type and the other two were 4039-Galileo Analytic Company Inc, all three had circular cones of 10 mm diameter.

All three channeltrons were used in a pulse counting, digital mode. The block diagram of the channeltron and counting system is shown in figure (3.10). To determine the pulse height distribution of a channeltron, the output of the amplifier was connected to a multichannel analyzer and the negative ion

beam directed to it. The pulse amplitude gives the estimate of the current gain of channeltron as a function of channel number of the multichannel analyzer. The channeltron voltage was adjusted to give a clear maximum in the pulse height distribution for different points of impact over most of the channeltron cone. The pulse heights from ions which go directly down the channel at the center of the cone are smaller than those which strike the cone itself.

If the channeltron is treated carefully, and not subjected to bad vacuum or contamination, the main factor governing its liftime is the total charge accumulation. For this reason great care was taken to never run a measurable beam current on to the cones. A protective metal plate was placed over the channeltrons to prevent accidental exposure during preliminary setting up procedures. This was moved aside during the measurements.

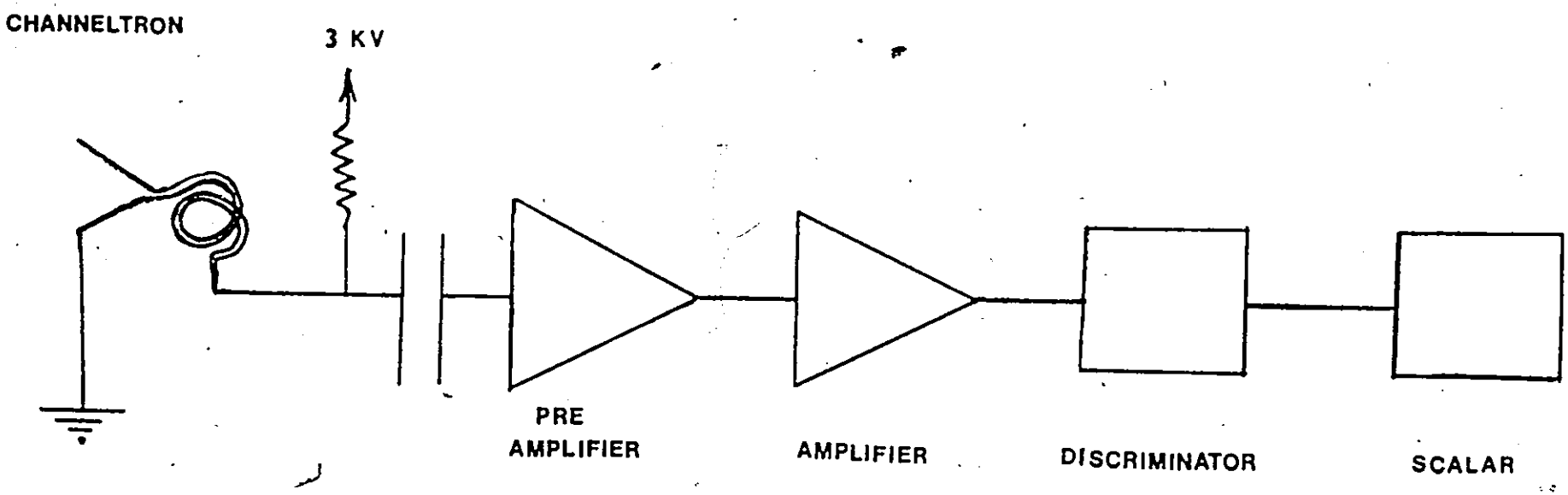

Figure 3.8: *Channeltron pulse counting system*

Chapter 4

Experimental Technique

4.1 Data Deduction

In the production of fluorine negative ions, higher anode voltages in the ion source was required and the adjustment was found to be more critical than with the chlorine beam. Measurements of fluorine-rare gas therefore were not taken below 20 keV due to the low beam intensity.

The raw data consisted of the counting ratio, N^+/N^0 for electron loss and N^-/N^0 for electron capture cross section at several different targets gas pressures. Each ratio and pressure reading provided one point on the graph. These points do not lie exactly on a line, because the ratio is of two digital numbers, each of which is subject to statistical fluctuations. Sufficiently large numbers of counts were obtained to give the ratio to a few percent at each

pressure. The cross section was calculated using the equations (2.19) and (2.20) where the raw data were N, the counting ratio, and the target pressure which is proportional to π.

A linear relation was obtained by plotting a graph of the right side of equations (2.19) and (2.20) as a function of the target pressure. The slopes of these graphs gave the cross sections, and the best estimates was made by employing the least squares fit method.

In order to satisfy the conditions that the correction terms could be completely ignored it would have been necessary to use targets so thin that the counting N^+ and N^- rates would have been very small, comparable to the background, so some corrections had to be made for multiple collisions. The target pressure range was chosen such that the correction terms were fairly small, a few percent.

A typical graph of the right side of equation (2.19) as a function of target pressure is shown in figure (4.1). A small intercept was found due to the collisions of the incident beam with the residual gas in a small region between the neutralizer and the target cell.

Figure 4.1: *Linear relation of the σ_{0-} cross section as a function of target gas pressure.*

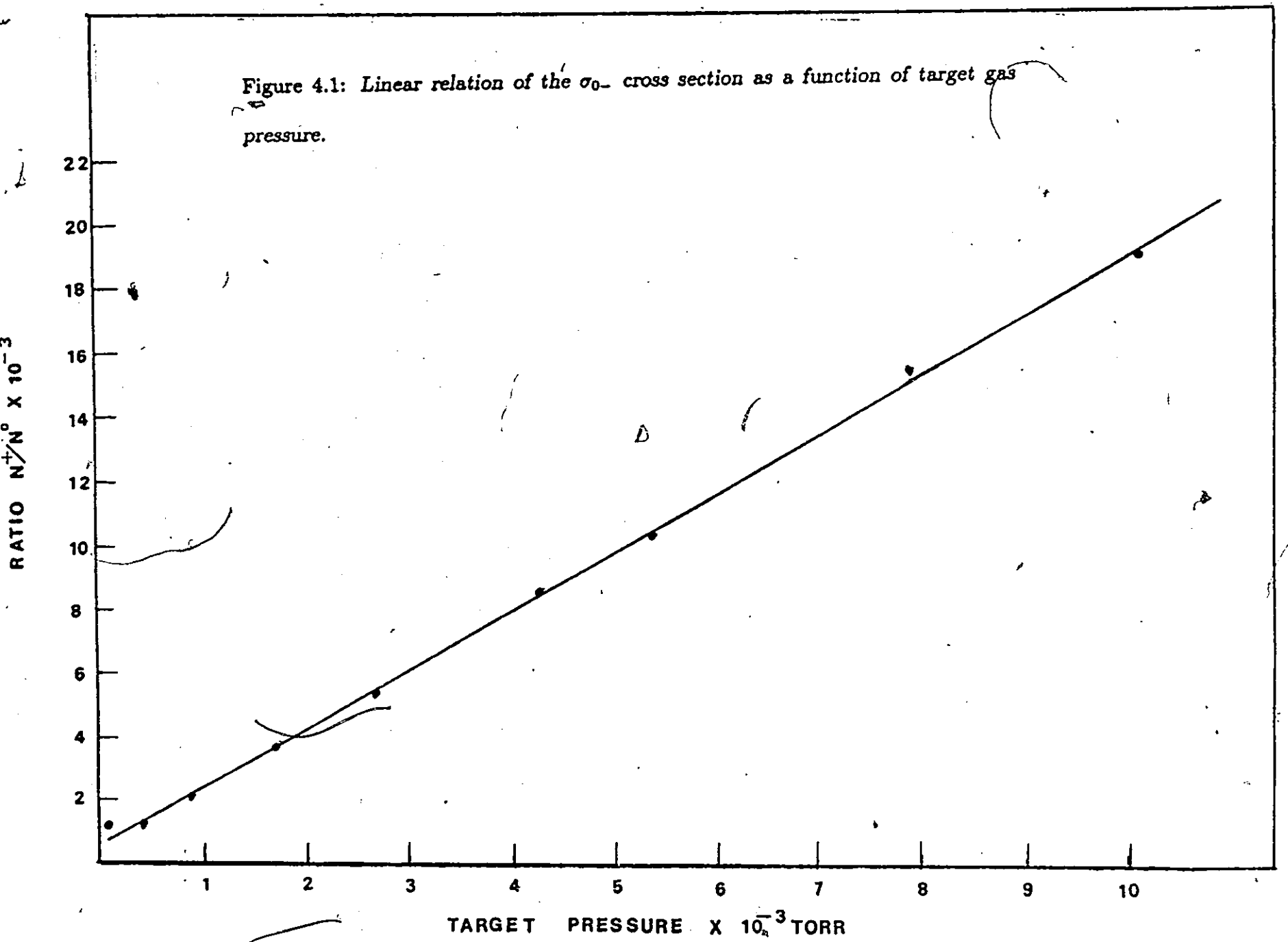

The cross sections in the correction were either obtained from publish measurements, or estimates were made. In fluorine rare-gas collisions, the single and double electron detachment cross sections were measured by Hird et al [2]. For double electron capture cross section σ_{+-} , the data of Fogel et al [3] was used. These exit up to 60 keV in oxygen-rare gas targets. The single electron capture cross section σ_{+0} was measured by Lookwood [4] in fluorine-rare gas collisions, except for the Kr and Xe targets. For Xe and Kr, their data was extrapolated to our energy range. Some of the cross sections were very small, for example the σ_{-2} cross sections, and these were ignored. The σ_{+2} were available for helium (Jorgensen et al [5]), and for neon and argon (Brackman and Fite [6]). These argon values were used as estimates of the krypton and xenon σ_{+2} cross sections.

In chlorine-rare gas collisions, the data of Fedorenko [7] for single electron capture, was used for all the rare gas targets. For the σ_{+0} cross section, the data of Witkower [8] was used, which exists only for Ne, Ar and Kr targets. Their Ne and Kr data was substituted for the He and the Xe targets respectively. A complete set of data on single and double electron detachment cross sections were measured by Hird et al [9] over the range of energies of the present measurements.

4.2 Analysis of Uncertainties

In order to assess the reliability of the present measurements, several possible sources of the systematic error were considered. The computer repeated the calculations with all the correction terms set to zero. The difference in the numerical values calculated in the two ways, was used as an estimate of the importance of the target thickness correction terms. If the difference exceeded 3%, then the higher pressure readings, where the target thickness terms are largest, were rejected from the data, and the cross section recalculated. The error in the cross sections, associated with the target thickness corrections, was estimated to be not more than 2% on any of the final results.

Another possible source of error was due to pressure measurements of the target cell by the capacitance manometer, since all cross sections are expressed in terms of the absolute target thickness, which is proportional to pressure. During the six hour run of the experiment, zero drifting in the manometer was noticed, the error of which was estimated to be 2% at higher pressures and less than 1% at lower gas pressures. The purity of the target gas was 99.9% which caused no serious error in the cross section measurements.

The channeltrons, each with a 1 cm diameter entrance aperture, were positioned side by side to collect all the particles scattered within a 2^0 half angle cone from the target center. The effective area of the channeltron was

found to be 9 mm from measurements of the pulse height distribution when the direct beam was traversed across the channeltron aperture. An additional uncertainty associated with particle loss at large angles was estimated to be not more than 1%. The combined errors from all sources add up to an estimate of 10% uncertainty on the cross section results.

Chapter 5

Results and Discussion

5.1 Fluorine-Rare Gas Collisions

The results obtained for the energy dependence of the negative ion production for fluorine on rare gas targets is shown in table (5.1). The general character of the cross section is illustrated in figure (5.1). The systematic errors associated with the data are estimated to be less than the error bars plotted on the graph. The previous data of Fogel et al [10] are shown in the same figure.

5.2 Negative Ion Production

The single electron capture cross section σ_{0-} are determined for fluorine collisions with He, Ne, Ar, Kr and Xe gas targets in the energy range from 10 to

110 keV.

The cross sections for heavy targets Ar, Kr and Xe increase and pass through a maximum. The maxima of these curves become narrow as the target mass increases, and the peaks are displaced towards lower energies for heavy targets respectively. The shift in the maxima is probably due to the competition between the stripping of the neutral fluorine beam with the removal of one electron and the ionization of the target atom. The σ_{0-} cross section in the He and Ne targets was found to be small at lower energies but shows a systematic rise in magnitude with the increase of the projectile energy.

There is no theoretical model for σ_{0-} cross section which could explain the detailed behavior of these curves. However the process during the collision certainly the transfer of an electron from the initial ground state of the target atom to projectile where it becomes the valence electron of the bound and stable negative ion. Massey adiabatic criterion [11] can predict roughly the positions of the energies of maxima of the σ_{0-} cross section. This model is applicable only when the initial and final states of the collision partners are well defined. The theoretical basis of the Massey calculation is described in Appendix. Since the neutral fluorine beam was obtained by neutralizing negative ions, we make the assumption that the beam is entirely in the ground state.

Table: 5.1: The cross section of the negative ion production σ_{O^-} of fluorine atom collision with rare gas atom.

	$\sigma_{O^-}(10^{-16}cm^2)$				
Energy (keV)	*He*	*Ne*	*Ar*	*Kr*	Xe
20.3	< .05	< .07	2.33	3.77	7.20
20.5	-	-	-	-	7.17
30.5	-	0.22	3.36	-	-
31.5	< .08	-	-	4.64	7.01
40.5	-	0.45	-	5.35	6.81
41.3	0.16	-	3.53	-	-
51.0	0.26	0.65	3.74	5.14	6.11
60.0	-	0.83	-	4.80	6.02
61.3	0.25	-	3.26	-	-
70.0	-	0.86	-	-	5.50
71.0	0.31	-	3.27	4.12	-
80.0	-	-	3.18	3.91	4.80
81.3	0.31	-	3.27	4.12	-
90.0	-	-	2.60	3.76	4.41
91.3	0.37	1.07	-	-	-
100.0	-	-	2.41	3.34	4.22
101.3	0.42	1.10	-	-	-
110.0	-	-	2.17	3.11	3.96
111.3	0.40	1.10	-	-	-

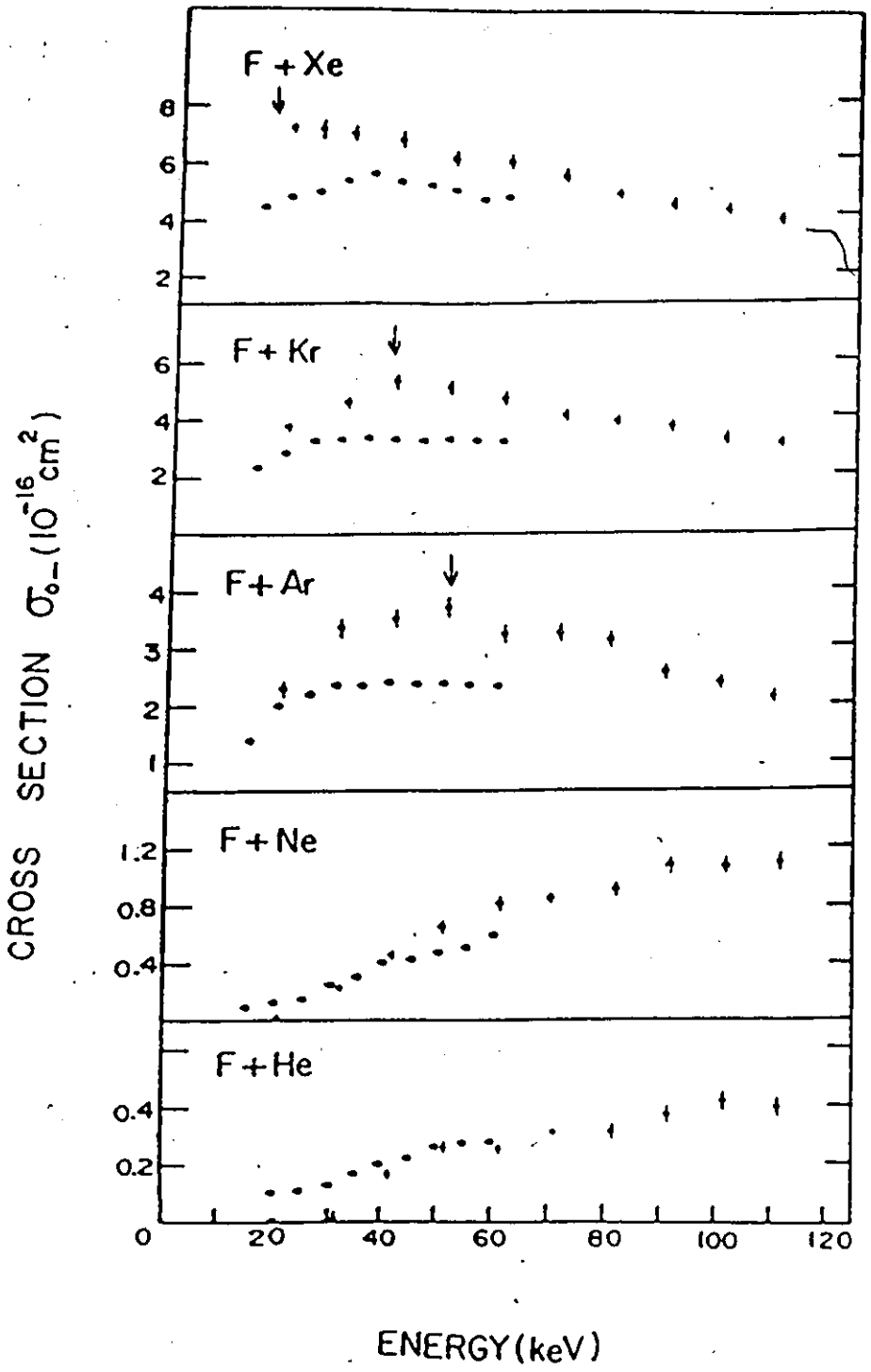

Figure 5.1: *The single electron capture cross section σ_{0-}. The open circles are the data of Fogel et al. The present data are shown by error bars. The arrows show the energy of the theoretical Massey maximum.*

Hasted and Lee [12] modified the Massey theory by adding the Coulomb and polarization interaction energies to the energy defect. Accordingly, the maximum cross section should occur near a projectile energy E_m such that

$$E_m^{1/2} = \frac{am^{1/2}|\Delta E|}{0.57} \tag{5.1}$$

where ΔE is the corrected energy defect described in Appendix, and a is the parameter which has an empirical value 6.7Å. The mass of the projectile is in atomic units and the energies are in eV. These theoretically estimated values for the energies at which the maximum of cross section should occur are given in table (5.2)

Fluorine	*ground state*	*metastable state*(12.7 *eV*)	Experiment
Target	Energy (keV)	Energy (keV)	Energy (keV)
He	294.0	11.68	> 110
Ne	298.3	25.55	> 110
Ar	56.61	170.0	56
Kr	42.20	198.70	42
Xe	20.02	259.40	< 20

Table 5.2: *The theoretical predictions and experimental values for the energies where the maximum* σ_{0-} *cross section of fluorine beam occurs.*

In the curves for the Ar , Kr and Xe targets, the measured maxima in the cross section curves appear at very closely similar energies to the Massey maxima predictions. For the helium and neon targets, the maximum are outside the range of measurements. The Massey theory, though a crude one, gives a probable explanation of the maxima on the curves.

Assuming that the fluorine beam is in the metastable state with excitation energy 12.7 eV, then a similar calculation predicted that the maximum cross section to be at energies below ours for helium, and rising with heavy targets to higher than our energies for xenon target. This opposite behavior of the experimental cross section indicates that the beam contained no significant proportion of metastable atoms.

5.3 Positive Ion Production

The results of the single electron loss cross section measurements are shown in table(5.3), and figure (5.2), where the cross sections are plotted as a function of the projectile energy. The σ_{0+} cross section was found to have the largest magnitude in He and the smallest in the Kr target. The cross section for all the rare gas targets, except for Ne, shows a systematic rise in magnitude with projectile energy. In the Ne target, above 90 keV, the cross section is almost energy independent. This may be due to the comparable mass of both the projectile and the target atom. The general behavior of the cross section results in light target suggests that the projectile ionization is the favorable process due to the low ionization potential of fluorine ($I.P = 17.4$ eV) as comparable to the He ($I.P = 24.58$ eV) and Ne ($I.P = 21.1$ eV) targets.

In Ar, the maximum cross section is nearly the same as the He and Ne cross section at 80 keV. This probably because of the comparable ionization potentials of Ar ($I.P = 15.76$ eV) and the fluorine atom. In heavy targets, where the ionization potentials are smaller than projectile atom, target ionization seems to occur for the Kr and Xe targets. Because of this the cross section has smaller magnitudes as compared to light targets.

	$\sigma_{o+}(10^{-16}cm^2)$				
Energy (keV)	*He*	*Ne*	*Ar*	*Kr*	Xe
20.3	1.04	1.44	0.31	0.14	< .10
25.0	-	-	-	-	0.15
30.5	- 7	1.61	0.67	-	-
31.5	1.31	-	-	0.31	0.30
40.5	-	1.73	-	0.67	0.38
41.3	1.38	-	0.92	-	-
51.0	1.45	1.95	1.08	0.88	0.61
60.0	-	1.83	-	0.95	0.77
61.3	1.41	-	1.10	-	-
70.0	-	1.88	-	-	0.86
71.0	1.61	-	1.18	1.04	-
80.0	-	-	1.33	1.13	1.04
81.3	1.64	0.91	-	-	-
90.0	-	-	1.38	1.28	1.08
91.3	1.88	1.89	-	-	-
100.0	-	-	1.53	1.35	1.21
101.3	1.92	1.86	-	-	-
110.0	-	-	1.68	1.04	1.45
111.3	1.96	1.86	-	-	-

Table: 5.3: The cross section of the positive ion production σ_{o+} of fluorine atom collision with rare gas atom.

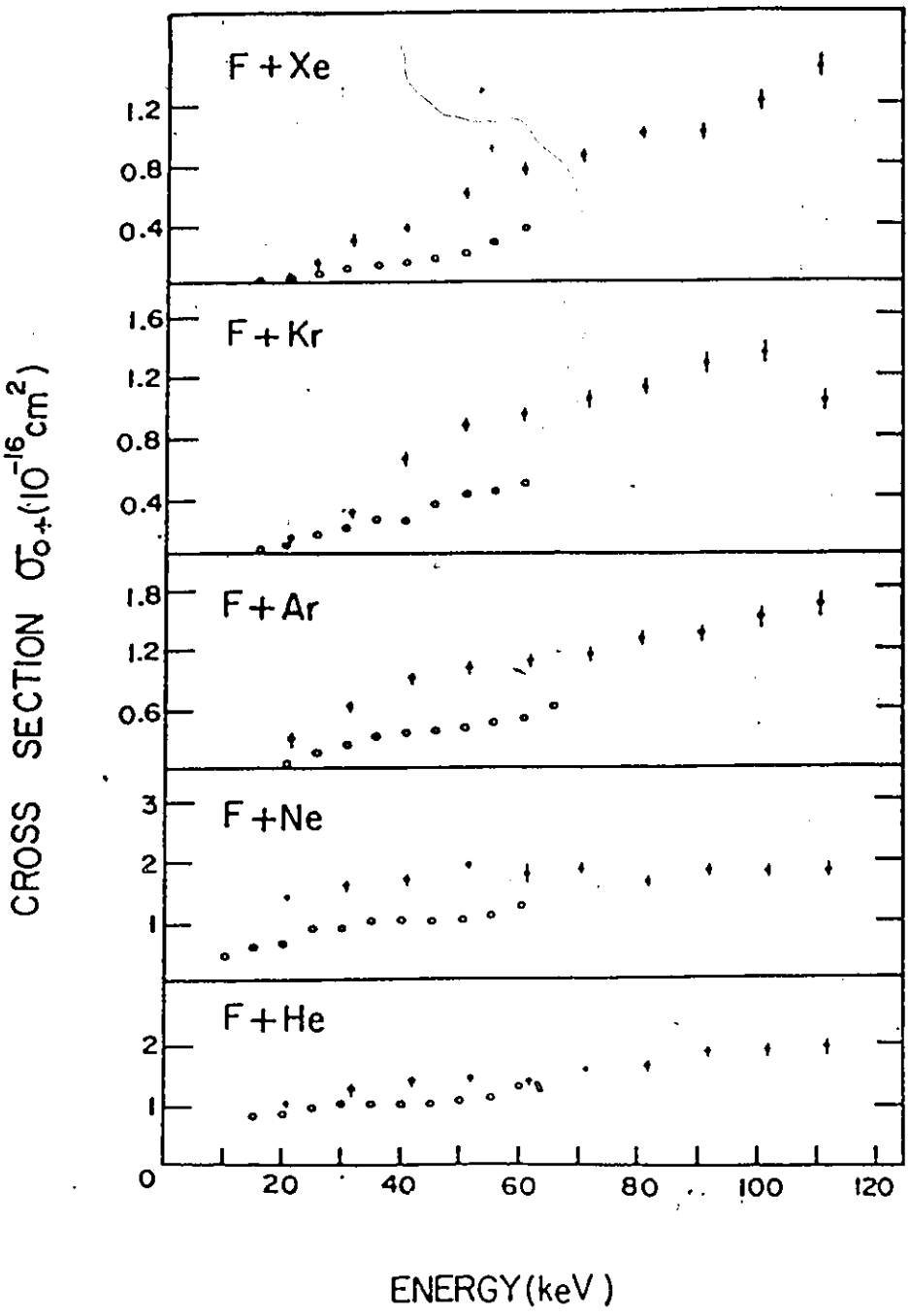

Figure 5.2: *The single electron loss cross section σ_{0+}. The open circles are the measurements of the Fogel et al. The present data are shown by the error bars.*

The present data on the ion pair production cross section were compared with the previous measurements of Fogel et al [8] in fluorine-rare gas collisions. Their data exist only up to 60 keV, and are shown in the same figures. It is apparent from the figures that the general behavior of the present curves is similar to that of the Fogel data, except for some differences in the magnitudes of the cross section results. The agreement of the present measurements is good for He and Ne targets. However, for the Ar target, their magnitude is less than the magnitude of present data by between 10% and 20%. In the Kr target, the difference is between 20% and 30%, and in the Xe target, it is between 25% and 30%. The differences are typically of the variations after found in these early measurements between absolute cross sections measured by different research groups. So that it is not safe to infer any physical significance to the difference between Fogel et al,s data and our more accurate results.

5.4 Chlorine-Rare Gas Collisions

5.5 Single Electron Capture

The results of the σ_{0-} cross section measurements are shown in table (5.4) and the values are plotted, on a logarithmic scale, as a function of beam energy in figure (5.3).

The behavior of the curves for Ar, Kr, and Xe targets shows that the cross section passes through a maximum and then decrease as the projectile energy increases. The maxima becomes sharp and narrow as the target mass decreases except, for the He and the Ne targets. The magnitudes of the cross section in light targets are found to be so small at lower energies, that it was only possible to set upper limits, as shown in figure and table.

The theoretical predictions for the energy of the Massey maxima were again calculated and are shown in table (5.5), assuming that the chlorine beam is either in the ground state or alternatively that it is in the metastable $(3p^4 4s, {}^4P_{\frac{1}{2}})$ state with excitation energy 8.9 eV. Under this assumption that the beam is entirely in the ground state, the cross section of light targets helium and neon should be small at lower energies since the Massey maxima is at much high energies. The agreement of the present measurements with the Massey maxima appears to be very good.

	$\sigma_{0-}(10^{-16}cm^2)$				
Energy (keV)	He	Ne	Ar	Kr	Xe
11	-	< .01	0.03	< .01	0.72
13	< .06	-	-	-	-
22	< .04	< .01	0.06	0.34	2.21
30	-	0.02	0.21	-	-
32	< .03	-	-	0.84	4.10
41	< .03	0.01	0.55	1.70	5.50
51	0.03	< .01	0.80	2.32	5.74
62	0.04	0.02	1.42	2.40	6.05
65.3	-	-	1.70	-	-
72	0.05	0.05	1.82	2.50	5.95
75.3	-	-	2.11	-	-
81	0.04	0.10	2.20	2.90	5.83
85.3	-	-	2.20	-	-
91	0.04	0.10	2.33	3.15	6.10
95.3	0.08	-	2.10	-	-
101	-	0.12	1.92	3.14	5.23
106	0.14	-	-	1.74	-
111	< .07	0.15	1.63	2.88	4.51

Table: 5.4 *The cross section for the negative ion production σ_{0-}, in a single collision between chlorine and rare gas atom.*

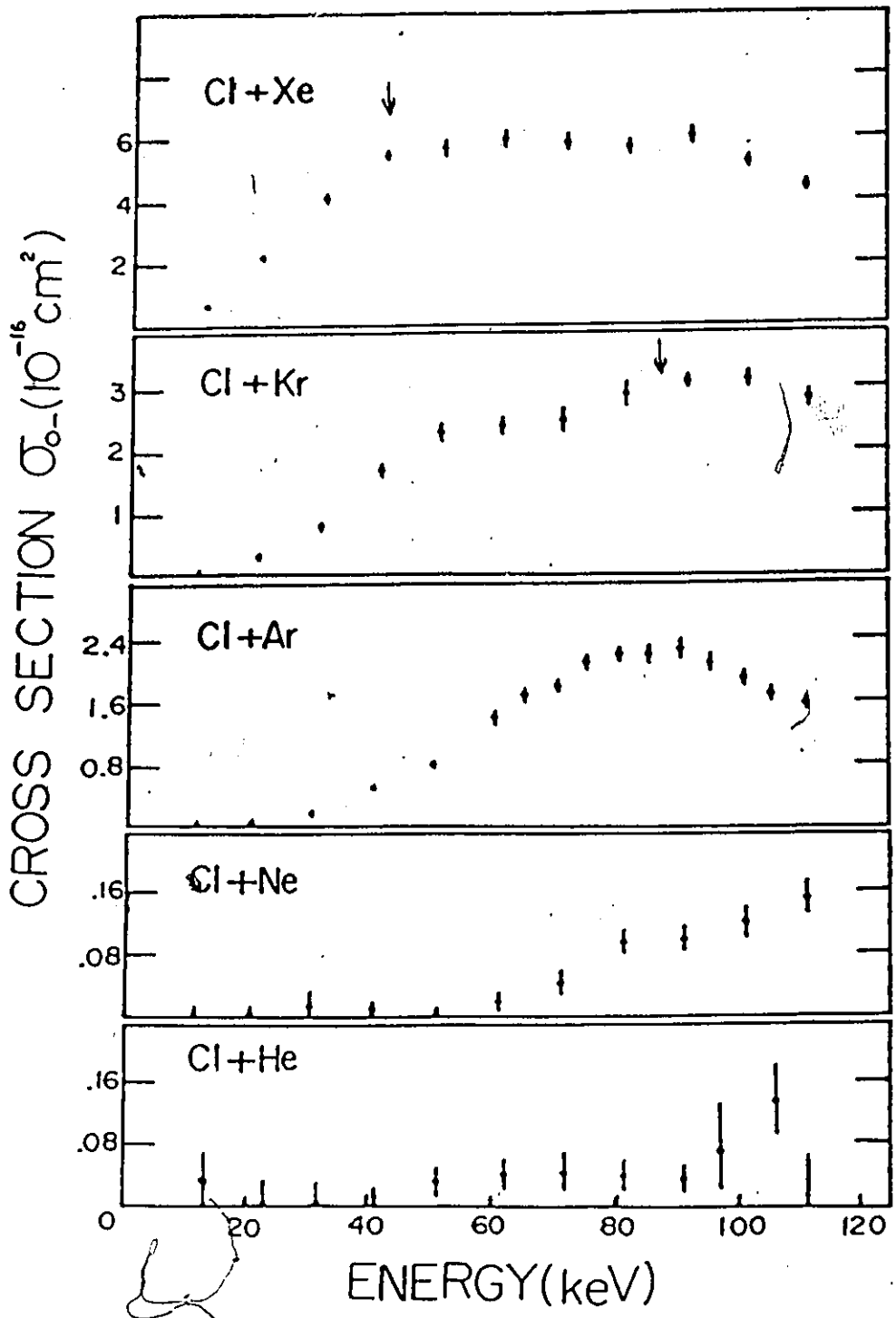

Figure 5.3: *The cross section for the negative ion production of chlorine-rare gas collision. The arrows show the energy of the theoretical Massey maximum.*

Chlorine	*ground state*	*metastable state*(8.9 *eV*)	Experiment
Target	*Energy*(*keV*)	Energy (keV)	Energy (keV)
He	702	45	> 110
Ne	516	9	> 110
Ar	129	71	91
Kr	88	108	90
Xe	41	179	45

Table 5.5: *The theoretical predictions and the experimental values for the energies where the maximum* σ_{0-} *cross section of chlorine beam is expected.*

As an extra check on the effect of the metastable atoms on present measurements, the polarity of the ion source was changed and the neutral chlorine beam was obtained by electron capture collisions with positive ions. The σ_{0-} and σ_{0+} cross sections were then remeasured in the Xe target with this beam at 45 keV and 80 keV energy range. The magnitudes of the cross sections were found to be 10% higher than the previous cross section values where the beam was obtained by neutralizing the accelerated negative ions in the neutralizer. This difference is within the statistical accuracy of cross section measurements, and is probably not significant.

Assuming that the neutral beam is in the ground state, the beam energy is close to the Massey maximum of the σ_{0-} cross section. But it is lower than the maximum for the metastable state of Cl atom. This means that the smaller cross section from the metastable state atoms in the beam could be expected. Therefore the measured cross section should be reduced rather than increased due to contamination of the beam by metastable atoms.

5.6 Single Electron Loss

The σ_{0+} cross section results are shown in table (5.6) and figure (5.4). The general trend of the cross section for all targets except for Ar, shows a systematic rise in magnitude with the projectile energy. Since the ionization potential of the chlorine atom is much smaller than the ionization potential of the He, Ne , Ar and Kr target, it suggests that projectile ionization is more likely to occur than target ionization. In Ar, the cross section increase and reaches a maximum at 90 keV, then it decreases as the beam energy increases. The projectile mass is smaller than the heavy targets and larger than He and Ne, but comparable to that of argon. This may be the reason that the cross section increases and decreases due to comparable mass of chlorine and argon atom.

In the Xe target, the cross section indicates that preferential target ionization may occur due to larger ionization potential of the chlorine as compared to the Xe target. This type of charge transfer cross section is not detected in our apparatus since the positive ions are then slow recoils rather than fast ions of approximately the beam energy. The behavior of the curve in Kr target suggests that both projectile and target ionization may be occurring, and that perhaps competition between target and projectile ionization, accounts for the small plateau in the energy range 50 keV to 65 keV.

	$\sigma_{0+}(10^{-16}cm^2)$				
Energy (keV)	He	Ne	Ar	Kr	Xe
11	-	0.30	0.84	0.28	0.30
13	0.06	-	-	-	-
22	1.19	0.83	1.61	1.40	0.82
30	-	1.41	2.25	-	-
32	1.87	-	-	1.94	1.55
41	2.17	1.90	2.80	2.55	2.40
51	2.50	2.36	3.40	2.86	2.31
62	2.87	2.67	3.55	2.74	2.61
65.3	-	-	3.20	-	-
72	3.31	3.00	4.10	2.85	2.75
75.3	-	-	4.25	-	-
81	3.30	3.11	5.15	3.20	2.81
85.3	-	-	4.80	-	-
91	3.60	3.30	5.21	3.56	3.10
95.3	3.00	-	4.60	-	-
101	-	3.50	4.12	3.62	3.26
106	3.25	-	4.11	-	-
111	3.51	3.41	3.75	4.05	3.45

Table: 5.6 *The cross section for the production of positive ion σ_{0+} in a single collision between chlorine and rare gas atom.*

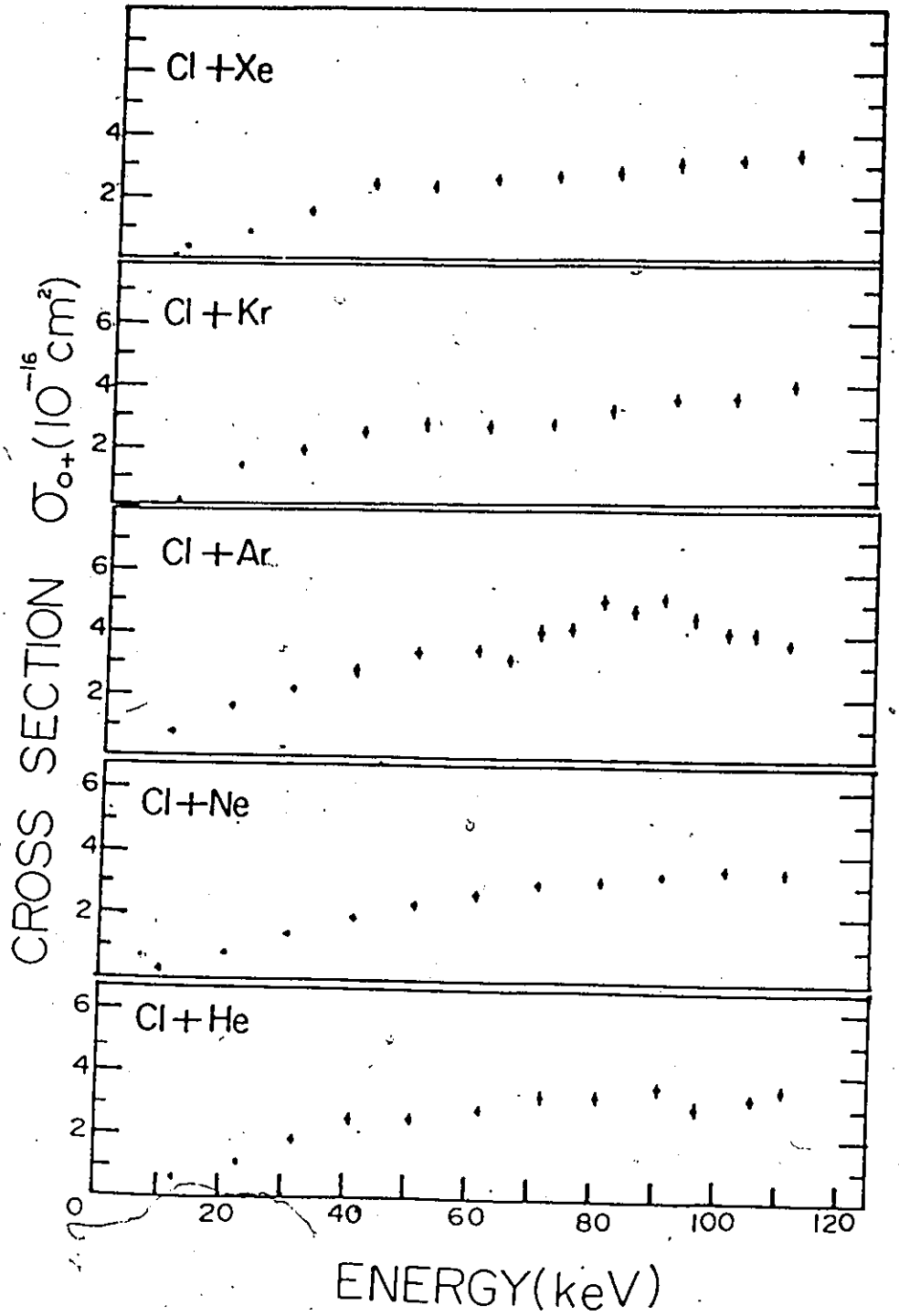

Figure 5.4: *The cross section for the positive ion production of chlorine-rare gas collision.*

Chapter 6

Appendix

6.1 Massey Criterion

According to this hypothesis, the transition between two states is most likely, when the collision time and the transition time are comparable. The duration of the collision can be expressed as $t = a/v$, where a is a distance of the order of atomic dimensions and v is the relative velocity of the colliding atoms. The quantum mechanical oscillation time between two states which differ by ΔE is

$$\Delta t = \frac{h}{|\Delta E|} \tag{6.1}$$

Massey associated the transition time with one half cycle of this quantum mechanical oscillation so that electrons have time to oscillate one way but

not back again between the two atoms. If the collision is very slow, the collision system are able to adjust themselves to the perturbation, the two states are orthogonal, and a transition is unlikely. In such a case the cross section will be small. With increasing velocity, the cross section would increase reaching a maximum value and then decrease when the interaction time becomes too short for the perturbation to change the wave funtions significantly and the transition is again unlikely. The combination of the collision time and the quantum mechanical time oscillation time gives an expression such that

$$E^{1/2} = \frac{am^{1/2}|\Delta E_\infty|}{2^{1/2}h} \tag{6.2}$$

which is called the Massey maximum rule for a charge transfer process. E is the collision kinetic energy.

Massey calculated the value of ΔE_∞ from the difference in internal energy of the atoms before and after the collision, when they are at infinite separation. Numerical values were obtained from the ionization potentials and electron affinities.

Hasted modified the Massey theory by making the assumption that the correct energy defect to use is not ΔE_∞, but ΔE_{corr}, the effective energy defect when they are at the separation at which transition occurs. This may be written as

$$\Delta E_{corr.} = \Delta E_\infty + E_c \tag{6.3}$$

where E_c is the Coulombs energy between the two ions. In other collision processes where one of the incident particle is an ion, the polarization energy was also included. They used a simple model to estimate the correction.

$$E_c = \frac{3}{2} e^2 \frac{r_1^2 - r_2^2}{r_1^3 - r_2^3} \tag{6.4}$$

where

$$r_{1,2} = k_{1,2} \left[Z_A^{\frac{2}{3}} + Z_B^{\frac{2}{3}} \right]^{\frac{1}{2}} \tag{6.5}$$

where the constants $k_{1,2}$ have values 1.44 and 0.48 respectively. Here Z_A is the atomic number of the projectile and Z_B is the atomic number of the target.

The Coulomb interaction energy for fluorine-helium collision is

$$E_c = 10.59 \quad eV \tag{6.6}$$

The uncorrected energy defect for the process

$$A + B \rightarrow A^- + B^+ - \Delta E_\infty \tag{6.7}$$

can be written in the form

$$\Delta E_\infty = E_A + E_{IP} \tag{6.8}$$

assuming all the colliding particles are in the ground states. where E_A is the electron affinity of particle A, and E_{IP} is the ionization potential of particle B. Using the ionization potential from table (6.1), one can easily find the energy defect for the electron transfer process.

Table 6.1: *The ionization potentials used in the calculations for the Massey maximum energies.*

Atom	I. P (eV)
He	24.58
Ne	21.59
Ar	15.76
Kr	14.00
Xe	12.13

On substitution into equation (6.3), the corrected energy defect ΔE_{corr} for fluorine-rare gas collisions are obtained. These are summarized in tables (6.2) and (6.3), when the fluorine beam is in the ground state or alternatively in the metastable state. Making use of these values, the maximum cross section can be predicted at the energy of Massey maximum.

In chlorine rare gas collisions, a similar calculation was performed and the theoretical predictions were estimated for chlorine beam in the ground state or alternatively in the metastable state which are summarized in tables (6.4) and (6.5).

Table 6.2: *Summary of the corrected energy defect for fluorine-rare gas collisions, when the fluorine atom is in the ground state.*

Atom	ΔE_∞ (eV)	E_c (eV)	ΔE_{corr} (eV)
He	-21.18	10.59	-10.59
Ne	-18.16	8.61	-9.55
Ar	-12.35	7.71	-4.64
Kr	-10.60	6.60	-4.00
Xe	-8.73	5.97	-2.76

Table 6.3: *Summary of the corrected energy defect for fluorine-rare gas collisions, when the fluorine atom is in the metastable state.*

Atom	ΔE_∞ (eV)	E_c (eV)	ΔE_{corr} (eV)
He	-8.48	10.59	2.11
Ne	-5.48	8.61	3.12
Ar	0.34	7.71	8.05
Kr	2.10	6.60	8.70
Xe	3.97	5.97	9.94

Table 6.4: *Summary of the corrected energy defect for chlorine-rare gas collisions, when the chlorine atom is in the ground state.*

Atom	ΔE_∞ (eV)	E_c (eV)	ΔE_{corr} (eV)
He	-20.96	9.00	-11.96
Ne	-17.96	7.68	-10.28
Ar	-12.44	7.02	-5.12
Kr	-10.38	6.15	-4.23
Xe	-8.51	5.64	-2.87

Table 6.5: *Summary of the corrected energy defect for chlorine-rare gas collisions, when the chlorine atom is in the metastable state.*

Atom	ΔE_∞ (eV)	E_c (eV)	ΔE_{corr} (eV)
He	-12.04	9.00	-3.04
Ne	-9.02	7.68	-1.34
Ar	-3.22	7.02	3.80
Kr	-1.46	6.15	4.69
Xe	0.41	5.63	6.04

Bibliography

[*] B. Hird, M. Bruyere, and S. Fafard. Can. J. Phys. 65, 735(1987).

[2] B. Hird and F. Rahman. Phys. Rev. A26, 3108(1982).

[3] Ya. M. Fogel, R. V. Mitin and A. G. Koval, Zh. Eksp. Theoret. Fiz. 31, 397(1956). [Sov. Phys. JEPT4, 359(1957)].

[4] G. J. Lookwood, Phys. Rev. A9, 1916(1954).

[5] T. Jorgensen, C. E. Kuyatt, W. W. Lang, D. C. Lorents and C. A. Sautter, Phys. Rev. 140 , 1481 (1965).

[6] R. T. Brackman and W. L. Fite, Technical Report No. AFWL-TR-68-96, United States Air Force Weapons Laboratory, Kertland Air Force Base, NM. 1968.

[7] N. V. Fedorenko, Zh. Tech. Fiz, 24, 769(1954).

[8] A. B. Witkower and H. B. Gilbody, Proc. Phys. Soc. 90, 353(1967).

[9] B. Hird and F. Rahman, J. Phys. B:16, 3581(1983).

[10] Ya. M. Fogel, V. A. Ankudiv, and D. V. Pilipenko. Zh. Eksp, Teor. Fiz.38, 26(1960).

[11] H. S. W. Massey, Rep. Prog. Phys. 12, 248(1949).

[12] J. B. Hasted and A. R Lee, Proc. Phys. Soc.79, 702(1962).

ABSTRACT

This thesis describes an experimental study of ion pair production and electron loss cross sections in neutral-neutral atom collisions. Fluorine and chlorine negative ion beams traversed a neutralizing cell. A clearing electric field removed the charged particles so that only a neutral beam entered a target cell, where the cross sections were measured. New equipment for the neutral beam production was constructed for the measurements of these cross sections. The neutralizer and the target gas cells were assembled as a unit and accurately machined, so that the entrance and the exit apertures of the system were exactly aligned. The cross section for the negative and positive ion production were measured in the laboratory projectile energy from 10 keV to 110 keV, under single collision conditions with rare gas targets. Some interesting behavior of the measured cross section for negative ion production in Ar, Kr and Xe was observed. The Massey adiabatic criterion was applied to predict the position of maxima of the σ_{0-} cross section and good agreement was found with our cross section results. All the measurements were made with an estimated experimental error of less than 10%.